UCRL-9489 Rev

# UNIVERSITY OF CALIFORNIA

## Ernest O. Lawrence Radiation Laboratory



BERKELEY, CALIFORNIA

## DISCLAIMER

UCRL-9489 Rev
Limited Distribution

UNIVERSITY OF CALIFORNIA
Lawrence Radiation Laboratory
Berkeley, California

Contract No. W-7405-eng-48

# S- AND P-WAVE INTERACTIONS OF $K^-$ MESONS IN HYDROGEN

Paul Nordin, Jr.

March 13, 1961

# S- AND P-WAVE INTERACTIONS OF $K^-$ MESONS IN HYDROGEN*

Paul Nordin, Jr.†

Lawrence Radiation Laboratory
University of California
Berkeley, California

March 13, 1961

## ABSTRACT

The experimental study of low-energy $K^-$-meson interactions in a hydrogen bubble chamber is continued and the energy range extended to a region that involves P waves.

Scattering and hyperon-production cross sections are measured at mean $K^-$-meson laboratory momenta of 300 Mev/c and 400 Mev/c.

Elastic-scattering angular distributions are obtained and, along with the values of the cross sections, indicate the presence of P waves.

Based on 289 observed decays, the measured $K^-$-meson lifetime is $1.31 \pm 0.08 \times 10^{-8}$ sec.

# I. INTRODUCTION

This work forms a small part of the general attack on the experimental investigation of the $K^-$-meson-nucleon interaction. Freden, Gilbert, and White[1] have summarized the published data in this field. Data from emulsion studies at the momenta considered in the present work have been published by the Berne group[2] and by Freden, Gilbert, and White.[1]

Preliminary results of this experiment have been reported at the 1959 Kiev Conference on High Energy Physics by Luis W. Alvarez,[3] and at American Physical Society meetings by Rosenfeld and by Nordin et al.[4,5] Eberhard et al. have reported on the charge-exchange reaction.[6]

The present work is intended to present the final values of the physical quantities obtained from this experiment and to describe the method of analysis. These results are summarized in Table I. A brief description of the experimental setup at the Bevatron is followed by an explanation of the scanning method used to obtain an unbiased sample of events. The sequence of operations involved in processing events is then described. This is followed by the data analysis and a discussion of the results.

# II. EXPERIMENTAL PROCEDURE

## A. Beam from the Bevatron

The experimental setup is adequately described elsewhere.[7] However a brief description of the beam is in order. The general setup is shown in Fig. 1. The Bevatron internal proton beam strikes a copper target, and particles emitted in the forward direction at about 450 Mev/c are bent through 90 deg in the Bevatron magnetic field. The particles exit through a 0.008-in. aluminum window in the Bevatron vacuum tank. They are then bent through about 45 deg in the C magnet M1 (this removes the dispersion introduced by the Bevatron fringe field), which is immediately followed by a single-element quadrupole magnet, focussing in the horizontal plane. The next element, which is the main reason for the success of the beam, is the Murray coaxial velocity spectrometer.[8] Following that is a collimator, a two-element quadrupole magnet, another collimator, and a 15-in. bubble chamber. The absorber used was copper, none being used for the 400 Mev/c run and 0.85 in. for the 300 Mev/c run.

The background-to-$K^-$ ratio was about 50 at 400 Mev/c and about 100 at 300 Mev/c. This difference presumably resulted from operation of the Bevatron on two generators at 400 Mev/c and on only one at 300 Mev/c (one generator had failed just prior to the 300 Mev/c run). Consequently it was necessary to use a different target position and a less efficient orbit in the Bevatron magnetic field.

## B. Scanning

The film was scanned by using the "pick-tooth" method, which is guaranteed to furnish an unbiased sample of events and also insure a high scanning efficiency. It takes advantage of the fact that a K meson at 400 Mev/c is about 1.9 times minimum ionization, while at 300 Mev/c the K meson is about 2.6 times minimum. The background tracks consisted largely of minimum-ionizing muons with about 15%

minimum-ionizing pions. This fact allows tentative identification of a track as a K meson before the K enters the fiducial volume. The fiducial volume is masked from view during the "picking" of the K track. The mask is then removed, and the entire length of the K is examined for interactions. If the K interacts, the type of interaction is recorded; if the K does not interact, it is noted down as a "K go-through" (KGT).

To insure a high scanning efficiency, scanners examined all KGT tracks a second time, looking especially for decays and small-angle scatters, since these are the types of events that are most likely to be missed. At 300 Mev/c, no new decays were found in the total KGT sample (about 1600 tracks), and only scatters in the forward region ($\cos\theta > 0.97$ c.m.) were found. The scanning efficiency is therefore very close to 100% at 300 Mev/c for all classes of events except very-small-angle scatters. These are discussed in the section on elastic scattering. At 400 Mev/c (about 2400 KGT), four additional decays and three additional scatters were found. The scatters are treated under the section on elastic scattering. The four decays were at large angles (27, 44, 63, and 90 deg) on the scanning table and could not possibly have been interpreted as a KGT. Therefore we assume that these were cases where the scanner put a check mark in the wrong column on the scan sheet. However, a further, very detailed examination of one-third of the KGT sample at 400 Mev/c revealed two decays that were indeed difficult to detect due to small angles and nearby background tracks. The correction for this effect is discussed in the section on the $K^-$ lifetime.

## C. Data Processing

Data processing, which begins immediately after scanning, can be divided into the following steps:

(a) Sketching. In this step, the event is re-examined and information is noted for the measuring step.

(b) Measuring. Film coordinates of the event are measured on "Franckenstein", the precision measuring device developed at the Lawrence Radiation Laboratory. Measuring is done on two views (four views are

available) for each track associated with the event, the two views used being determined by the orientation of the track. The film coordinates are punched on IBM cards for subsequent use by digital computers.

(c) Reconstruction of Event. This step is accomplished by the digital-computer program PANG.[9] The program calculates dip, azimuth, and momentum at both ends of a track, including the errors and their correlations.

(d) Kinematic Fitting. This step is accomplished by the digital-computer program KICK.[10] The input is the output of PANG. The constraints of energy and momentum conservation are applied to the measured variables, and these variables are adjusted by a least-squares fit. The output is the adjusted kinematical variables characterizing the event, along with the quantity $\chi^2$ representing the goodness of fit.

Each event undergoes this process. The K-meson decays and the K-meson zero-prong events ($K_\rho$) are not kinematically fitted. These types of events are accepted if the PANG momentum and angles are appropriate to the particular beam momentum setting.

# III. ANALYSIS

## A. Path-Length Measurement

The major contribution (about 90%) to the path length is the sample of K mesons that go through the chamber (KGT). A smaller contribution is from the K mesons that decay or interact in the fiducial volume.

The straightforward approach used for the determination of path length was to measure on Franckenstein approximately one-third of the KGT sample at each momenta. This measured sample was then sent through a digital-computer program (PATH) which (a) tested for certain acceptability criteria the azimuth, dip, and position of each track, and (b) computed the track length lying in the fiducial volume and the momentum at its entrance plane. The momentum distribution of the accepted tracks at the entrance plane is shown in Figs. 2 and 3 for the two momentum values.

The average path length, $\bar{L}$, contributed by each accepted KGT is then calculated and used to extrapolate to the total sample of KGT. A small correction to the total sample was made assuming the same percentage of acceptability failures in the unmeasured sample.

The path length contributed by K mesons that interact or decay in the fiducial volume is calculated by assuming that they interact or decay, on the average, $(1/2)\ \bar{L}$ through the fiducial volume.

The mean momentum at the entrance plane was calculated from a weighted average of the measured momenta. The weight factor for each momenta is the inverse square of the measurement error. This mean momentum was then used to calculate the mean momentum at a distance of $(1/2)\ \bar{L}$ into the fiducial volume. These momentum values are 299.8 Mev/c and 400.1 Mev/c, with errors on the mean of about 0.5 Mev/c.

The momentum spread of the beam from the Bevatron can be calculated approximately by unfolding the measurement errors from the observed histrogram. Assuming each measurement has the same error,

we have

$$\delta\, p^2(\text{beam}) = \delta\, p^2(\text{histogram}) - \delta\, p^2(\text{measurement}).$$

The conversion factor from number of events, N, to a cross section is

$$a = A/(\rho N_0 L)$$

and

$$\sigma = aN,$$

where A is the atomic weight of hydrogen, $N_0$ is Avogadro's number, $\rho$ is the density of liquid hydrogen under bubble chamber operating conditions (0.0586 $g/cm^3$), and L is the path length in centimeters.

Table II summarizes the quantities for each momentum value.

Since the identification of a KGT is subjective, the question of pion or muon contamination in the KGT sample is valid. It is shown in Appendix I that this contamination is less than 1%.

## B. Elastic Scattering

### 1. General Considerations in Detecting Small-Angle Scatters

The efficiency for the detection of small-angle scatters depends on (a) $\Theta$, the laboratory angle between the incident and scattered K meson, (b) $\phi$, the angle between the normal to the scattering plane and the direction to a camera lens, and (c) the size of the projected angle $\Theta_p = \Theta \sin\phi$. Angle $\Theta_p$ is the larger angle in either of the two views used to scan the track length, and the size of this angle is a measure of the likelihood of detection. A correction to the data using $\Theta_p$ as a criterion has the disadvantage of obscuring the physically interesting quantities in the center of mass. Furthermore, the validity of such a correction is not obvious, since recoil protons, which become visible even for small $\Theta_p$, enhance the likelihood of detection.

A simple approach to the problem considers only the c.m. quantities and imposes a cutoff on the accepted c.m. angle $\theta$. Details of this method follow the next section.

### 2. Evidence for High Detection Efficiencies

300 Mev/c. The second examination of the KGT sample (about 287 meters of track length) described under the section on Scanning revealed five scatters. Figure 4a shows the distribution of events in the forward region, with these five events cross-hatched. Since the four events with $\cos\theta > 0.99$ are probably single-Coulomb scatters, they do not enter the calculation of the nuclear-scattering cross section.

400 Mev/c. Three scatters were found during a second examination of the KGT sample (about 489 meters of track length). Figure 4b shows the distribution of events in the forward region, with these three events cross-hatched.

The event that was missed on the first examination at $\cos\theta = 0.86$ has a $\Theta_p$ value of 8 deg in one view and 4 deg in the other and a recoil proton track 0.7 cm long. Therefore the missing of this event on the first examination is considered to be a rare instance of poor scanning technique.

From this evidence one feels confident of the detection efficiency for small-angle scatters. It will be shown in the next section that all of

the physical quantities determined in the elastic-scattering analysis vary essentially within their statistical errors for various values of the cutoff angle.

3. Analysis of Elastic Scattering

The analysis is carried out in the center of mass. Only S and P waves are assumed to be present ( $\lambda$, the c.m. De Broglie wave length over $2\pi$, is 0.8 fermi at 400 Mev/c and 1 fermi at 300 Mev/c. The K-meson Compton wave length over $2\pi$ is 0.4 fermi).

The solid angle is divided into six regions. The detection efficiency is assumed to be unity for all six regions except the forward-scattering region. The detection efficiency in this region is assumed to be unity from $x_1 = 2/3 \leqslant \cos\theta \leqslant x_2$ and zero from $x_2 \leqslant \cos\theta \leqslant 1.0$. The average detection efficiency, $\bar{\epsilon}$, can be calculated from

$$\bar{\epsilon} = \frac{\int_{x_1}^{x_2} (A_1 + A_2 x + A_3 x^2)\, dx}{\int_{x_1}^{1.0} (A_1 + A_2 x + A_3 x^2)\, dx}, \qquad (1)$$

where

$$\frac{d\sigma}{d\Omega} = A_1 + A_2 x + A_3 x^2, \qquad (2)$$

and $x = \cos\theta$. The $A_i$ and the associated error matrix $\overline{\delta A_i \delta A_j}$ are calculated by solving the nonlinear maximum-likelihood equations by an iterative procedure, using the method described by Crawford.[11] Since the $A_i$ are initially unknown, the starting value $\bar{\epsilon}$ is assumed to be given by $\bar{\epsilon} = \int_{x_1}^{x_2} dx \,/\, \int_{x_1}^{1.0} dx$. (The calculation is empirically independent of the initial value of $\bar{\epsilon}$). This inital value of $\bar{\epsilon}$ is used to calculate the $A_i$. From (1), $\bar{\epsilon}$ is calculated. This value of $\bar{\epsilon}$ is used to recalculate the $A_i$. The process is continued until $\bar{\epsilon}$ and the $A_i$ remain constant.

The calculations are done for several values of the cutoff $x_2$. A comparison of the results for the different values of $x_2$ is made in Figs. 5 and 6 and Table III. A discussion of these comparisons follows.

300 Mev/c. Figure 5 shows the fitted curves for various values of $x_2$ in the forward region only. The backward regions are almost identical for the different values of $x_2$. The dotted curves represent the statistical errors on the curve for the typical case $x_2 = 0.978$. In Table III, N(observed) is the number of events actually found in the region $x_1 \leqslant \cos\theta \leqslant x_2$, and N(expected) is the number of events predicted by the fitted curve (i.e., proportional to $\int_{x_1}^{x_2} d\sigma$). The forward-scattering cross section shows the largest variation as a function of $x_2$. This is to be expected, since the forward scattering is sensitive to the number of events found in the forward region.

It is felt that the curve for $x_2 = 0.978$ is the most reasonable choice at 300 Mev/c. The full curve with its errors is shown in Fig. 7. The numbers of events observed in each region are indicated. Table IV gives the parameters characterizing the curve.

400 Mev/c. The curve for $x_2 = 0.97$ represents the data best. This curve is plotted in Fig. 8. Table IV summarizes the pertinent quantities.

### C. Charge-Exchange Scattering

The charge-exchange-scattering cross section was measured by counting the number of $K_1^0$ mesons that decayed into two charged pions, and applying a correction for the neutral decays.[12] No escape correction was made.

300 Mev/c. One $K_1^0$ decay was found. The corresponding cross section is given in Table I.

400 Mev/c. Five $K_1^0$ decays were found. The corresponding cross section is given in Table I.

### D. Charged-Hyperon Production

The cross-section measurements consist of counting the number of events accepted and using the conversion factor from events to millibarns given in Table II.

300 Mev/c. At this momentum there were nine $\Sigma^-$ and ten $\Sigma^+$ hyperons produced. The cross sections are given in Table I. The distribution of the pion in the center of mass is shown in Fig. 9.

400 Mev/c. At this momentum there were eleven $\Sigma^-$ and eighteen $\Sigma^+$ hyperons produced. The cross sections are given in Table I. The distribution of the pion in the center of mass is shown in Fig. 10.

There were no cases of two pions being produced with a charged $\Sigma$ at either 300 or 400 Mev/c.

### E. Neutral-Hyperon Production

The combined cross sections for production of all neutral hyperons is given in Table I. This measurement is based on the number of visible decays of the $\Lambda$ into a proton and a negative pion. There were five of these decays at 300 Mev/c and thirteen at 400 Mev/c. A correction for the number of neutral decays is applied.[12] A further escape correction of 2% is made.

The individual cross sections for production of $\Lambda$ and $\Sigma^0$ are of considerable importance. A maximum-likelihood calculation of the ratio $x = \Lambda/(\Lambda + \Sigma^0)$ has been made, by using a larger sample of charged

$\Lambda$ decays (the larger sample results primarily from decays that were not found in the "pick-tooth" scan). Details of this calculation are given in Appendix II. The results are:

| P (Mev/c) | x | $(\Sigma^0+\pi^0)$ (mb) | $(\Lambda+\pi^0)$ (mb) |
|---|---|---|---|
| 300 | $0.64 \pm 0.20$ (7) | $2.7 \pm 1.9$ | $4.8 \pm 2.6$ |
| 400 | $0.54 \pm 0.14$ (18) | $6.3 \pm 2.4$ | $5.4 \pm 2.2$ |

The production of a neutral hyperon and two neutral pions has been neglected.

Two examples of $\Lambda\pi^+\pi^-$ and one of $\Sigma^0\pi^+\pi^-$ were observed at 400 Mev/c. One $\Lambda\pi^+\pi^-$ and no cases of $\Sigma^0\pi^+\pi^-$ were observed at 300 Mev/c. The cross sections for these processes are given in Table I.

## F. Reaction Cross Sections

The reaction cross section is defined to include all processes except elastic scattering. It can be calculated in two ways: (a) by summing all the partial cross sections, or (b) by counting all events and converting to a cross section. The difference in the two methods is that (a) ignores the zero-prong ($K_\rho$) events (but includes corrections for them) and (b) includes the zero-prong events. The zero-prong events are cases of neutral particles being produced but not being observed because of neutral decay or escape from the chamber.

Both methods give the same result at 400 Mev/c (18 $K_\rho$), but at 300 Mev/c there are an unusually large number of $K_\rho$ (12). These have been carefully examined and satisfy all the qualitative and quantitative tests for acceptance. Therefore method (b) yields the more reliable result. Results of the two methods are compared in the following table:

| P (Mev/c) | $\sigma_r$, method a (mb) | $\sigma_r$, method b (mb) |
|---|---|---|
| 300 | 28.6 ± 6.0 | 34.9 ± 5.7 |
| 400 | 37.3 ± 5.8 | 37.3 ± 4.5 |

The existence of this minor anomaly implies that one or more of the cross sections for production of neutral particles at 300 Mev/c ($\bar{K}^0$, $\Lambda$, or $\Sigma^0$) has been underestimated.

The total cross sections given in Table I result from the sum of $\sigma_r$ (computed by method b) and the elastic cross section.

## G. $K^-$-Meson Lifetime

The $K^-$-meson lifetime is obtained by dividing the observed proper time by the observed number of decays. The observed proper time is obtained from the path-length measurement L by

$$T_{obs} = M_K L/P_K,$$

where $M_K$ is the mass of the $K^-$ meson and $P_K$ is the mean momentum of the $K^-$-meson beam.

There were 134 decays observed at 300 Mev/c and at 400 Mev/c there were 155 decays observed. However two of these 155 decays at 400 Mev/c were found only after very careful examination of one-third of the KGT sample. In order to correct for this effect, it is assumed that there are four more such decays in the KGT sample which was not measured. This gives a total of 293 decays at both momenta. The observed time from both momenta is $3.85 \times 10^{-6}$ sec. The mean life is thus

$$\tau_{K^-} = (1.31 \pm 0.08) \times 10^{-8} \text{ sec.}$$

This is to be compared with the $K^+$ lifetime of $(1.224 \pm 0.013) \times 10^{-8}$ sec.[13] One may also compare this with the measurements of the $K^-$ lifetime: $(1.38 \pm 0.24) \times 10^{-8}$ sec,[1] $(0.95\ ^{+0.36}_{-0.25}) \times 10^{-8}$ sec,[14] $(1.60 \pm 0.30) \times 10^{-8}$ sec,[15] $(1.25 \pm 0.11) \times 10^{-8}$ sec,[16] $(1.17 \pm 0.12) \times 10^{-8}$ sec,[17] and $(1.25\ ^{+0.22}_{-0.17}) \times 10^{-8}$ sec.[18] The weighted average of these values is approximately $1.24 \pm 0.07 \times 10^{-8}$ sec.

## IV. DISCUSSION OF RESULTS

The elastic-scattering angular distribution with S and P waves can be written

$$\frac{d\sigma}{d\Omega} = \frac{1}{4k^2}\left\{\left|S + (2P_3+P_1)\cos\theta\right|^2 + \left|P_1 - P_3\right|^2 \sin^2\theta\right\} . \quad (1)$$

The optical theorem in this notation involves the real parts of the amplitudes:

$$\frac{k^2\sigma_T}{2\pi} = \mathrm{Re}\,(S + P_1 + 2P_3), \quad (2)$$

where S, $P_1$, and $P_3$ are the scattering amplitudes in the S wave, P wave $J = 1/2$, and P wave $J = 3/2$, respectively. Each amplitude is the sum of two isospin amplitudes for $I = 0$ and $I = 1$. The total cross section is denoted $\sigma_T$ and k is the c.m. wave number of the K meson. Equation (1) has eleven real parameters which completely describe the elastic and charge-exchange scattering. The present data are clearly insufficient to determine these parameters. Even if one neglects the isotopic-spin dependence of S, $P_1$, and $P_3$, the data are insufficient to determine these quantities. One can, however, obtain an estimate of two of these complex amplitudes under various assumptions on the third. These estimates will perhaps prove useful in further detailed calculations when more data are available.

Quantitative calculations at 300 Mev/c would be inappropriate in view of the scanty nature of the data. Qualitatively, the data are consistent with pure S wave, although some P wave cannot be excluded. If the P wave is neglected, the data indicate that the proton is almost a perfectly absorbing black body to the $K^-$ meson (that is, the scattering and reaction cross sections are both approximately $\pi\lambda^2$).

At 400 Mev/c Table IV shows that $A_3$ (the coefficient of $\cos^2\theta$) is large, so that the elastic scattering differential cross section must have non-zero $P_3$, but is consistent with a variety of assumption on S and $P_1$. We consider the following: (a) $P_1 = P_3$; (b) $P_1 = 0$; (c) $S = 0$; and (d) $S = 0$, $P_1 = 0$. The solutions are given in Table V. Only the relative sign of Im(S) versus Im($P_3$) is determined and Im(S) has been chosen arbitrarily negative. In case (c), only the magnitudes and the included angle are determined, and Im($P_3$) has been set arbitarily to zero. In case (d), the sign of Im($P_3$) is undetermined.

Table VI gives the solutions for $A_3$ varied by one standard deviation, $A_1$ changed according to the correlation coefficient in Table IV, and $A_2$ allowed to vary freely within about one standard deviation (the correlation coefficient is very small). The columns for the $A_i$ give the variation in standard deviations.

These calculations show that the S-wave contribution to the total cross section at 400 Mev/c is a maximum of about 45% [the central value is about 31% in case (a) and about 7% in case (b)].

## V. ACKNOWLEDGMENTS

The pleasant task of acknowledging aid to the author is complicated by the large number of persons responsible. A debt of gratitude is owed to Drs. Luis Alvarez, Arthur Rosenfeld, Frank Solmitz, and Robert Tripp. Messrs. Ron Ross, William Humphrey, and Peter Berge are largely responsible for the very excellent digital-computer data-analysis programs.

Thanks are due to many scanners, in particular to Mr. Jacob M. Neufeld for his tireless efforts.

The author is grateful for the experimental facilities provided by the Bevatron staff and for the efforts of the bubble-chamber operating crew headed by Messrs. Robert Watt and Glenn Eckman.

Valuable criticism was supplied by Dr. Robert G. Glasser.

# VI. APPENDICES

## Appendix A. Delta-Ray Cross Sections[20]

A K meson of 470-Mev/c momentum can produce delta rays having ranges from zero to 3.2 cm in liquid hydrogen. A $\pi$ meson of 400 Mev/c momentum can produce delta rays having ranges from zero to 34 cm. The cross section for such a $\pi$ meson to produce a delta ray having a range between 3.2 and 34 cm is 208 mb.

The measured KGT sample (one-third of the total sample) was examined for delta rays having a range equal to or greater than 3.2 cm. Had one such delta ray been found, it would have indicated a contamination of 0.86 % pions or muons. Since none were found, one may conclude that the probability of a p% pion or muon contamination is $e^{-p/0.86}$.

During the search for long delta rays, it was desirable to check detection efficiencies. This was accomplished by counting on the KGT tracks the number of delta rays having a range greater than 0.5 cm. The theoretical cross section for this process is 1.25 barns. The measurement yielded 1.19 ± 0.07 barns, in good agreement with the theoretical value.

## Appendix B. Maximum-Likelihood Calculation

The kinetic energy of a $\Lambda$ in the $K^-$-p center of mass is assumed to be unique if it is a direct $\Lambda$, and uniformly distributed between $T_1$ and $T_2$ if from a $\Sigma^0$. This is illustrated in Fig. 11.

The likelihood function is

$$L(x, T_i, \sigma_i) = \prod_{i=1}^{N} f(x, T_i, \sigma_i),$$

where

$$f(x, T_i, \sigma_i) = \frac{x}{\sqrt{2\pi}\sigma_i} e^{-\frac{(T_i - T_\Lambda)^2}{2\sigma_i^2}} + \frac{(1-x)}{\sqrt{2\pi}\,\sigma_i (T_2 - T_1)} \int_{T_1}^{T_2} e^{-\frac{(T_i - T)}{2\sigma_i^2}}\, dT.$$

Here $T_i$ is the experimental kinetic energy of the $\Lambda$ in the center of mass, $\sigma_i$ is the error assigned to $T_i$, and x is the ratio of the number of direct $\Lambda$ to N, the total number of $\Lambda$. The other quantities are

$$T_\Lambda = (p_\Lambda^2 + M_\Lambda^2)^{1/2} - M_\Lambda$$

where $$p_\Lambda^2 = \frac{w^4 - 2w^2(M_\Lambda^2 + M_\pi^2) + (M_\Lambda^2 - M_\pi^2)^2}{4w^2},$$

$$w^2 = M_K^2 + M_P^2 + 2M_P W_K,$$

$$W_K^2 = P_K^2 + M_K^2,$$

$P_K$ = $K^-$ laboratory momentum,

$$T_1 = (1/M_\Sigma)\left[(p_\Sigma^2 + M_\Sigma^2)^{1/2} w_{\Lambda\Sigma} - p_\Sigma p_{\Lambda\Sigma} - M_\Sigma M_\Lambda\right],$$

$$T_2 = (1/M_\Sigma)\left[(p_\Sigma^2 + M_\Sigma^2)^{1/2} w_{\Lambda\Sigma} + p_\Sigma p_{\Lambda\Sigma} - M_\Sigma M_\Lambda\right],$$

$$p_\Sigma^2 = \frac{w^4 - 2w^2(M_\Sigma^2 + M_\pi^2) + (M_\Sigma^2 - M_\pi^2)^2}{4w^2},$$

$$p_{\Lambda\Sigma} = \frac{M_{\Sigma}^2 - M_{\Lambda}^2}{2M_{\Sigma}},$$

$$w_{\Lambda\Sigma} = (p_{\Lambda\Sigma}^2 + M_{\Lambda}^2)^{1/2},$$

and

$$M_{\pi} = \pi^0 \text{ mass.}$$

The likelihood function is calculated as a function of x by using the experimental quantities $P_K$ and $T_i$ and their errors and correlations. The results are illustrated in Fig. 12 for 300 Mev/c and Fig. 13 for 400 Mev/c.

## FOOTNOTES

*This work was done under the auspices of the U. S. Atomic Energy Commission.

†Present address: Aeronutronic Division of Ford Motor Company, Newport Beach, California.

1. S. C. Freden, C. Gilbert, and R. S. White, Phys. Rev. 118, 564, (1960).
2. Y. Eisenberg, W. Koch, E. Lohrmann, M. Nikolić, M. Schneeberger, and H. Winzeler, Nuovo cimento 9, 745 (1958).
3. Luis W. Alvarez, The Interactions of Strange Particles, UCRL-9354, August 11, 1960. This is the only source for this material at present.
4. A. H. Rosenfeld, Bull. Am. Phys. Soc. 3, 363 (1958).
5. P. Nordin, A. H. Rosenfeld, F. T. Solmitz, R. D. Tripp, and M. B. Watson, Bull. Am. Phys. Soc. 4, 288 (1959).
6. P. Eberhard, A. H. Rosenfeld, F. T. Solmitz, R. B. Tripp, and M. B. Watson, Phys. Rev. Letters 2, 312 (1959).
7. N. Horwitz, J. J. Murray, R. R. Ross, and R. D. Tripp, 450 Mev/c $K^-$ and $\bar{p}$ Beams at the Northwest Target Area of the Bevatron Separated by the Coaxial Velocity Spectrometer, UCRL-8269, June 1958.
8. Joseph J. Murray, A. Coaxial Static-Electromagnetic Velocity Spectrometer for High Energy Particles, UCRL-3492, May 1957.
9. A. H. Rosenfeld, in Proceedings of the International Conference on High Energy Accelerators and Instrumentation (CERN, Geneva, 1959), pp. 533-541.
10. A. H. Rosenfeld and J. N. Snyder, Digital-Computer Analysis of Data from Bubble Chambers. IV. The Kinematic Analysis of Complete Events, UCRL-9098, February 16, 1960. Submitted to Review of Scientific Instruments.
11. Frank S. Crawford, Jr., An Easy Iterative Solution for All Maximum Likelihood "Histogram" Problems, UCID 173, January 6, 1958 (unpublished). Specific use was made of MALISOAP-3, an IBM 650 program.

12. F. S. Crawford, Jr., M. Cresti, R. L. Douglass, M. L. Good, G. Kalbfleisch, M. L. Stevenson, and H. K. Ticho, Phys. Rev. Letters 2, 266 (1959).
13. W. H. Barkas and A. H. Rosenfeld, Data for Elementary-Particle Physics, UCRL-8030, March 20, 1958.
14. E. L. Lloff, G. Goldhaber, S. Goldhaber, J. E. Lanutti, F. C. Gilbert, C. E. Violet, R. S. White, D. M. Fournet, A. Pevsner, D. Ritson, and M. Widgoff, Phys. Rev. 102, 927 (1956).
15. Y. Eisenberg, W. Koch, E. Lohrmann, M. Nikolić, M. Schneeberger, and H. Winzeler, Nuovo cimento 8, 663 (1958).
16. Walter H. Barkas, in Proceedings of the Seventh Annual Rochester Conference on High Energy Nuclear Physics, 1957 (Interscience Publishers, Inc., New York, N. Y., 1957), Chap. VIII, p. 30.
17. H. C. Burrowes, D. O. Caldwell, D. H. Frisch, D. A. Hill, D. M. Ritson, and R. A. Schluter, Phys. Rev. Letters 2, 119 (1959).
18. Morris A. Nickols, The Lifetime and Decay Modes of Negative K Mesons, UCRL-8692 (Thesis), September 1959.
19. Massimiliano Ferro-Luzzi, $K^-$-p Hydrogen Chamber Experiments, paper presented at Conference on Strong Interactions, University of California, Berkeley, December 1960; see Bull. Am. Phys. Soc. 5, 516 (1960).
20. See Frank S. Crawford, Use of Delta Rays to Determine Particle Velocities, UCID-241, November 20, 1957 (unpublished). See also idem., Phys. Rev. 117, 1119 (1960).

Table I. Summary of the partial-cross-section measurements, integrated over all angles. The number of events on which the cross section is based are indicated in parentheses.

| Reaction | Cross section, $\sigma$ (mb) | |
|---|---|---|
| | 300 Mev/c | 400 Mev/c |
| $K^- + p \rightarrow K^- + p$ | 44.5±6.4 (48) | 38.9±4.7 (69) |
| $\rightarrow \bar{K}^0 + n$ | 2.7±2.7 ( 1) | 8.1±3.7 ( 5) |
| $\rightarrow \Sigma^- + \pi^+$ | 8.3±2.8 ( 9) | 6.0±1.8 (11) |
| $\rightarrow \Sigma^+ + \pi^-$ | 9.2±2.9 (10) | 9.9±2.3 (18) |
| $\rightarrow \begin{cases} \Lambda + \pi^0 \\ \Sigma^0 + \pi^0 \end{cases}$ | 7.5±3.4 ( 5) | 11.7±3.3 (13) |
| $\rightarrow \Lambda + \pi^+ + \pi^-$ | 0.9±0.9 ( 1) | 1.1+0.8 ( 2) |
| $\rightarrow \Sigma^0 + \pi^+ + \pi^-$ | no events | 0.5±0.5 ( 1) |
| Total cross section - | 79.4±8.6 (86)[a] | 76.2±6.5 (137)[a] |
| $\pi \lambda^2$ | 34.1 | 20.1 |

[a]Note that these numbers are not the sum of the individual events. This point is discussed in the text.

Table II. Summary of path-length measurements

| | 300 Mev/c | 400 Mev/c |
|---|---|---|
| $\delta p$(measured) (Mev/c) | 10.4 | 12.4 |
| $\delta p$(histogram) (Mev/c) | 21.5 | 18.6 |
| $\delta p$(beam) (Mev/c) | 18.8 | 13.9 |
| $\bar{L}$(cm) | 21.1 | 21.6 |
| KGT path length (meters) | 287 | 488 |
| Path length from K mesons that decay or interact (meters) | 24 | 32 |
| L (meters) | 311 | 520 |
| Conversion factor $\alpha$ from events to cross section (mb) | 0.919 | 0.549 |

Table III. Summary of elastic-scattering quantities as a function of $x_2$

| $x_2$ | N(observed) | N(expected) | $\bar{\epsilon}$ | $\frac{d\sigma}{d\Omega}(0)$ (mb/sr) | $\sigma$ (mb) |
|---|---|---|---|---|---|
| | | 300 Mev/c | | | |
| 0.93 | 6 | 5.0 | 0.825 | 2.1 ± 1.5 | 43.2 + 6.4 |
| 0.94 | 6 | 5.0 | 0.853 | 2.0 ± 1.5 | 43.1 + 6.4 |
| 0.95 | 7 | 5.8 | 0.870 | 2.5 ± 1.6 | 44.0 ± 6.4 |
| 0.96 | 7 | 5.9 | 0.898 | 2.4 ± 1.5 | 43.8 ± 6.4 |
| 0.97 | 7 | 5.9 | 0.925 | 2.3 ± 1.5 | 43.6 ± 6.4 |
| 0.978 | 8 | 6.7 | 0.942 | 2.7 ± 1.6 | 44.5 ± 6.4 |
| 0.98 | 9 | 7.4 | 0.945 | 3.2 ± 1.6 | 45.4 ± 6.5 |
| 0.99 | 10 | 8.2 | 0.971 | 3.5 ± 1.7 | 46.2 ± 6.5 |
| | | 400 Mev/c | | | |
| 0.94 | 9 | 11.2 | 0.787 | 4.6 ± 1.3 | 36.8 ± 4.6 |
| 0.95 | 10 | 12.1 | 0.820 | 4.8 ± 1.3 | 37.1 ± 4.6 |
| 0.96 | 12 | 13.7 | 0.854 | 5.3 ± 1.3 | 38.1 ± 4.7 |
| 0.97 | 14 | 15.3 | 0.889 | 5.7 ± 1.4 | 38.9 ± 4.7 |
| 0.98 | 14 | 15.5 | 0.926 | 5.5 ± 1.3 | 38.5 ± 4.6 |
| 0.99 | 15 | 16.4 | 0.962 | 5.6 ± 1.3 | 38.8 ± 4.6 |

Table IV. Parameters characterizing the curves

| Parameter | 300 Mev/c | 400 Mev/c |
|---|---|---|
| $\frac{d\sigma}{d\Omega}(0)$ | 2.7 ± 1.6 | 5.7 ± 1.4 |
| $\sigma$ | 44.5 ± 6.4 | 38.9 ± 4.7 |
| $A_1$ | 4.017 | 1.755 |
| $A_2$ | 0.118 | -0.093 |
| $A_3$ | -1.430 | 4.024 |
| $\overline{\delta A_1 \delta A_1}$ | 0.686 | 0.231 |
| $\overline{\delta A_2 \delta A_2}$ | 0.733 | 0.531 |
| $\overline{\delta A_3 \delta A_3}$ | 3.266 | 1.987 |
| $\overline{\delta A_1 \delta A_2}$ | -0.005 | -0.005 |
| $\overline{\delta A_1 \delta A_3}$ | -1.182 | -0.469 |
| $\overline{\delta A_2 \delta A_3}$ | 0.059 | 0.028 |

Table V. Scattering amplitudes for elastic scattering at 400 Mev/c.

| Case | Re(S) | Im(S) | Re($P_1$) | Im($P_1$) | Re($P_3$) | Im($P_3$) |
|---|---|---|---|---|---|---|
| (a) | 0.58 | -0.87 | 0.44 | 0.29 | ($P_3 \equiv P_1$) | |
| (b) | 0.14 | -0.49 | 0 | 0 | 0.88 | 0.26 |
| (c) | 0 | 0 | 1.32 | 0.15 | 0.29 | 0 |
| (d) | 0 | 0 | 0 | 0 | 0.95 | 0.40 |

Table VI. Scattering amplitudes for elastic scattering at 400 Mev/c with experimental quantities varied

| Case | Re(S) | Im(S) | Re($P_1$) | Im($P_1$) | Re($P_3$) | Im($P_3$) | $A_3$ | $A_1$ | $A_2$ |
|---|---|---|---|---|---|---|---|---|---|
| (a) | 0.72 | -0.61 | 0.39 | 0.47 | $P_3 \equiv P_1$ | | +1.0 | -0.69 | 0 |
| | 0.50 | -0.80 | 0.46 | 0.40 | | | +1.0 | -0.69 | -1.0 |
| | 0.83 | -0.45 | 0.35 | 0.50 | | | +1.0 | -0.69 | +1.0 |
| | | | No solution | | | | 0 | 0 | -1.0 |
| | 0.88 | -0.57 | 0.34 | 0.41 | | | | | +1.0 |
| | 0.86 | -0.76 | 0.35 | 0.25 | | | -1.0 | +0.69 | +1.8[a] |
| (b) | | | No solution for any $A_2$ | | | | +1.0 | -0.69 | – |
| | | | No solution | | | | 0 | 0 | -1.0 |
| | 0.37 | -0.34 | 0 | 0 | 0.76 | 0.51 | | | +1.0 |
| | 0.57 | -0.66 | 0 | 0 | 0.66 | 0.32 | -1.0 | +0.69 | +1.6[a] |
| (c) | 0 | 0 | 0.92 | 0.83 | 0.48 | 0 | +1.0 | -0.69 | +0.1 |
| | | | No solution | | | | -1.0 | +0.69 | +0.1 |
| (d) | 0 | 0 | 0 | 0 | 0.95 | 0.40 | +0.20 | -0.14 | +0.1 |

[a]Only solution.

## FIGURE LEGENDS

Fig. 1. Schematic diagram of the system.

Fig. 2. Momentum distribution at entrance plane to fiducial volume at 300 Mev/c. Shaded events do not contribute to the path length.

Fig. 3. Momentum distribution at entrance plane to fiducial volume at 400 Mev/c. Shaded events do not contribute to the path length.

Fig. 4. Distribution of elastic scatters in forward region only at (a) 300 Mev/c and (b) 400 Mev/c. Cross-hatched events were found on the second examination of the track length.

Fig. 5. Variation of curves fitted to the 300-Mev/c elastic scattering as a function of the cutoff $x_2 = \cos\theta$ (c.m.). The dotted curves are the statistical errors. Only the forward region is shown.

Fig. 6. Variation of curves fitted to the 400 Mev/c elastic scattering as a function of the cutoff $x_2 = \cos\theta$(c.m.). The dotted curves are the statistical errors. Only the forward region is shown.

Fig. 7. Fitted curve for elastic-scattering angular distribution at 300 Mev/c. Events observed in each interval are indicated. The dotted curve represents the statistical errors. $|\text{Im } f(0)|^2$ as obtained from the optical theorem is indicated.

Fig. 8. Fitted curve for elastic scattering at 400 Mev/c. Observed events in each interval are indicated. The dotted curve represents the statistical errors. $|\text{Im } f(0)|^2$ as obtained from the optical theorem is indicated.

Fig. 9. Angular distribution of the pion produced with a $\Sigma$ hyperon at 300 Mev/c. (a) $\Sigma^-(\pi^+)$; (b) $\Sigma^+(\pi^-)$.

Fig. 10. Angular distribution of the pion produced with a $\Sigma$ hyperon at 400 Mev/c. (a) $\Sigma^-(\pi^+)$; (b) $\Sigma^+(\pi^-)$.

Fig. 11. Assumed theoretical distribution of $\Lambda$ in $K^-p$ center of mass.

Fig. 12. Relative probability for a particular value of x, as a function of x. 300 Mev/c, seven events.

Fig. 13. Relative probability for a particular value of x, as a function of x. 400 Mev/c, 18 events.

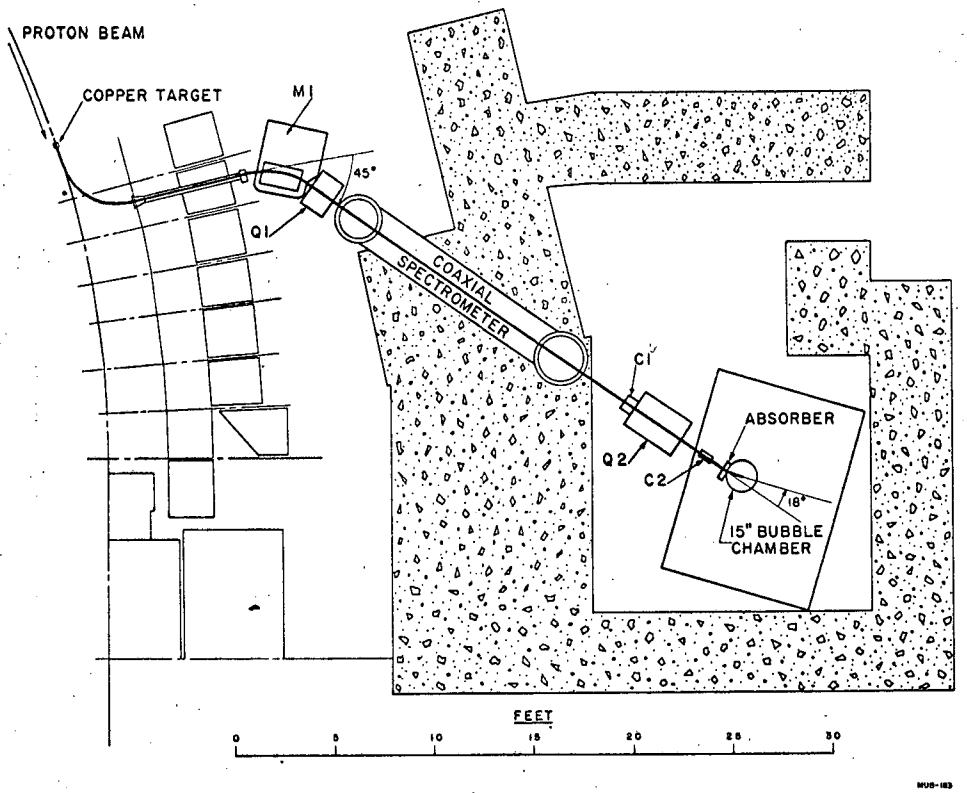
PROTON BEAM
COPPER TARGET
M1
45°
Q1
COAXIAL SPECTROMETER
C1
Q2
C2
ABSORBER
18°
15" BUBBLE CHAMBER
FEET
0
5
10
15
20
25
30

Fig. 1

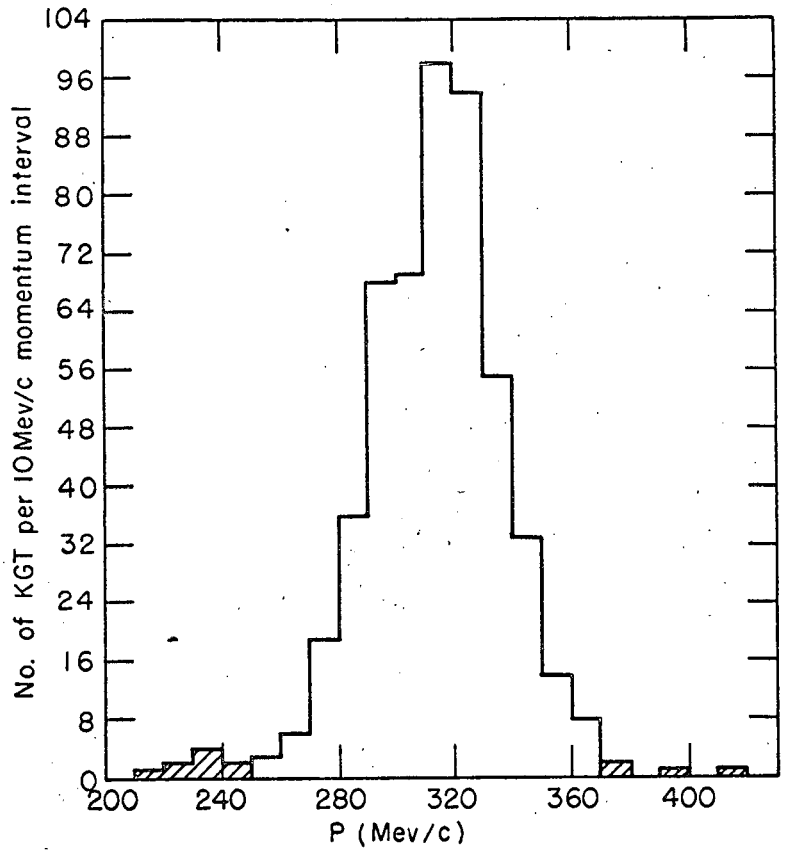
No. of KGT per 10 Mev/c momentum interval
104
96
88
80
72
64
56
48
40
32
24
16
8
0
200
240
280
320
360
400
P (Mev/c)
MU-22293

Fig. 2

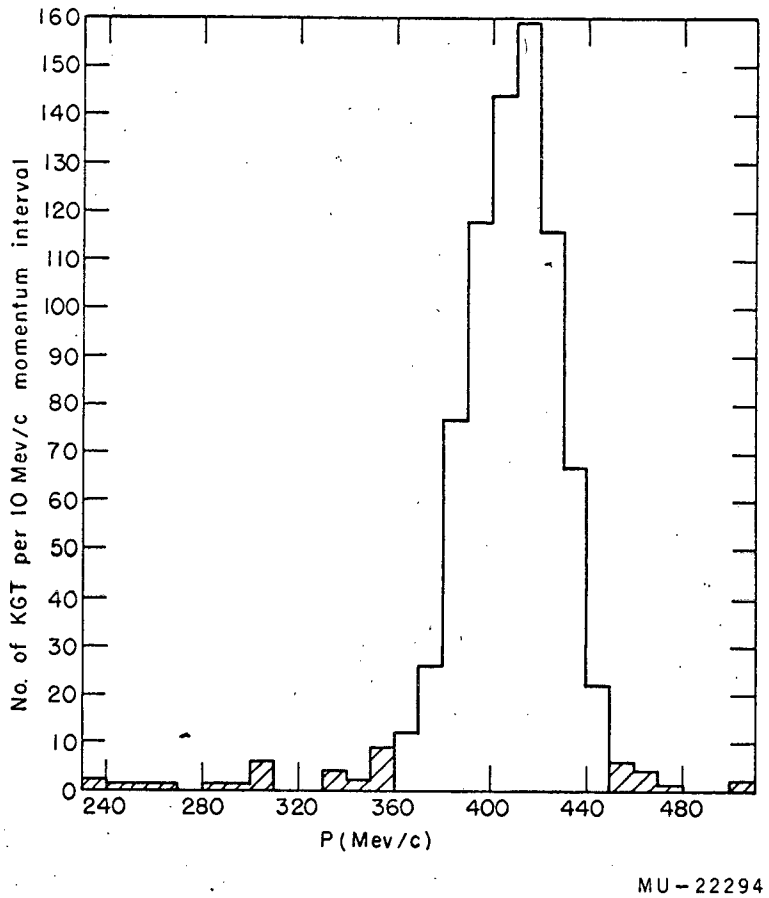
No. of KGT per 10 Mev/c momentum interval
160
150
140
130
120
110
100
90
80
70
60
50
40
30
20
10
0
240
280
320
360
400
440
480
P (Mev/c)
MU-22294

Fig. 3

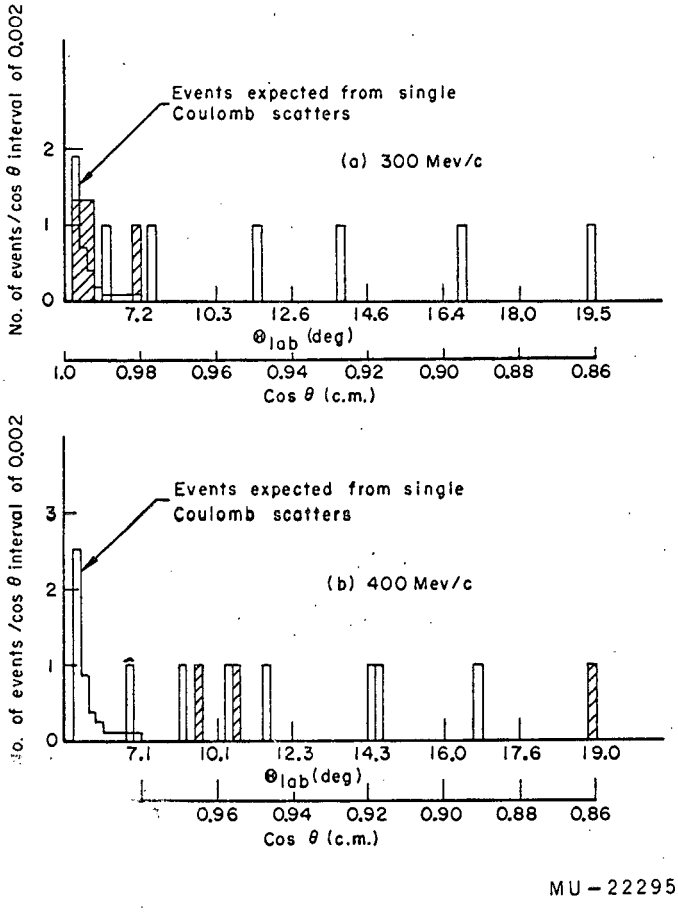
No. of events/cos θ interval of 0.002
Events expected from single Coulomb scatters
(a) 300 Mev/c
0
1
2
7.2
10.3
12.6
14.6
16.4
18.0
19.5
θlab (deg)
1.0
0.98
0.96
0.94
0.92
0.90
0.88
0.86
Cos θ (c.m.)
No. of events /cos θ interval of 0.002
Events expected from single Coulomb scatters
(b) 400 Mev/c
0
1
2
3
7.1
10.1
12.3
14.3
16.0
17.6
19.0
θlab (deg)
0.96
0.94
0.92
0.90
0.88
0.86
Cos θ (c.m.)
MU-22295

Fig. 4

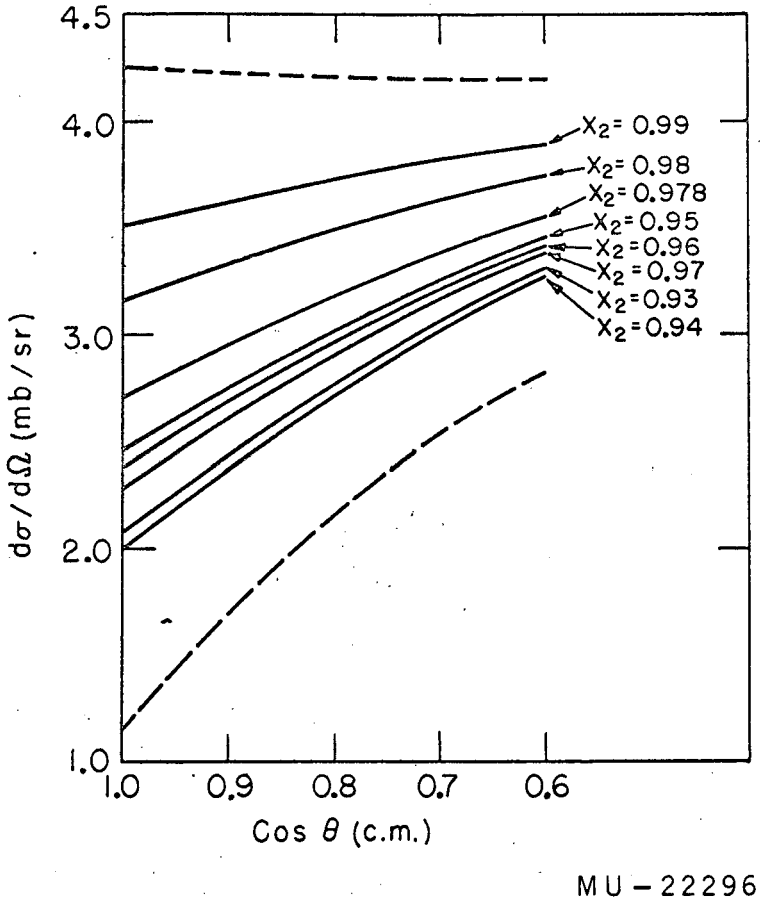
4.5
4.0
3.0
2.0
1.0
dσ/dΩ (mb/sr)
X2= 0.99
X2= 0.98
X2= 0.978
X2= 0.95
X2= 0.96
X2= 0.97
X2= 0.93
X2= 0.94
1.0
0.9
0.8
0.7
0.6
Cos θ (c.m.)
MU-22296

Fig. 5

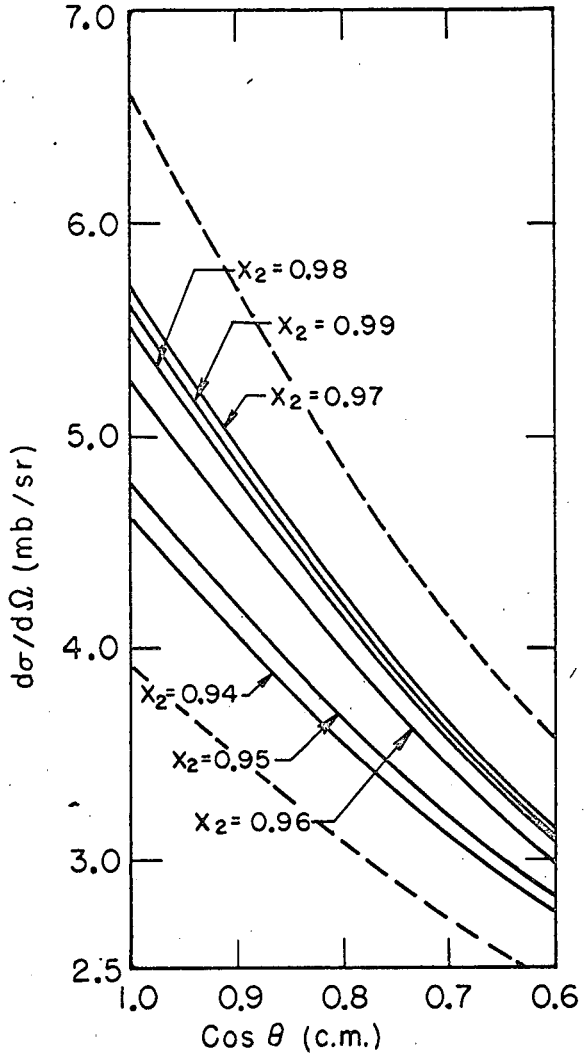
7.0
6.0
5.0
4.0
3.0
2.5
dσ/dΩ (mb/sr)
X2 = 0.98
X2 = 0.99
X2 = 0.97
X2 = 0.94
X2 = 0.95
X2 = 0.96
1.0
0.9
0.8
0.7
0.6
Cos θ (c.m.)
MU-22297

Fig. 6

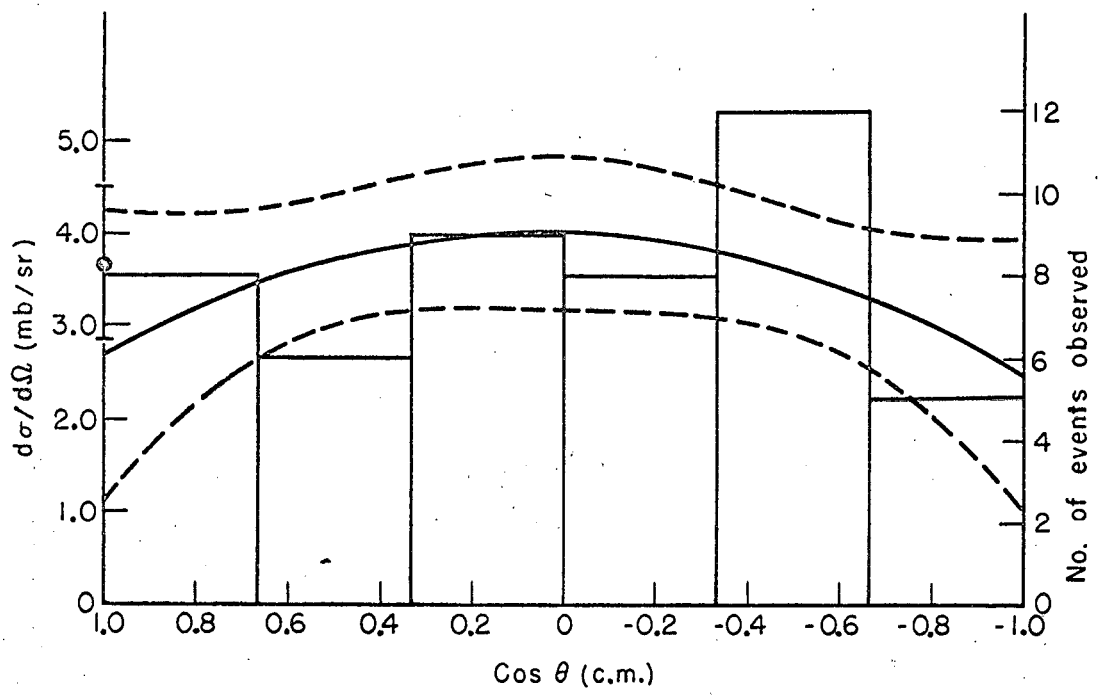


MU-22298

Fig. 7

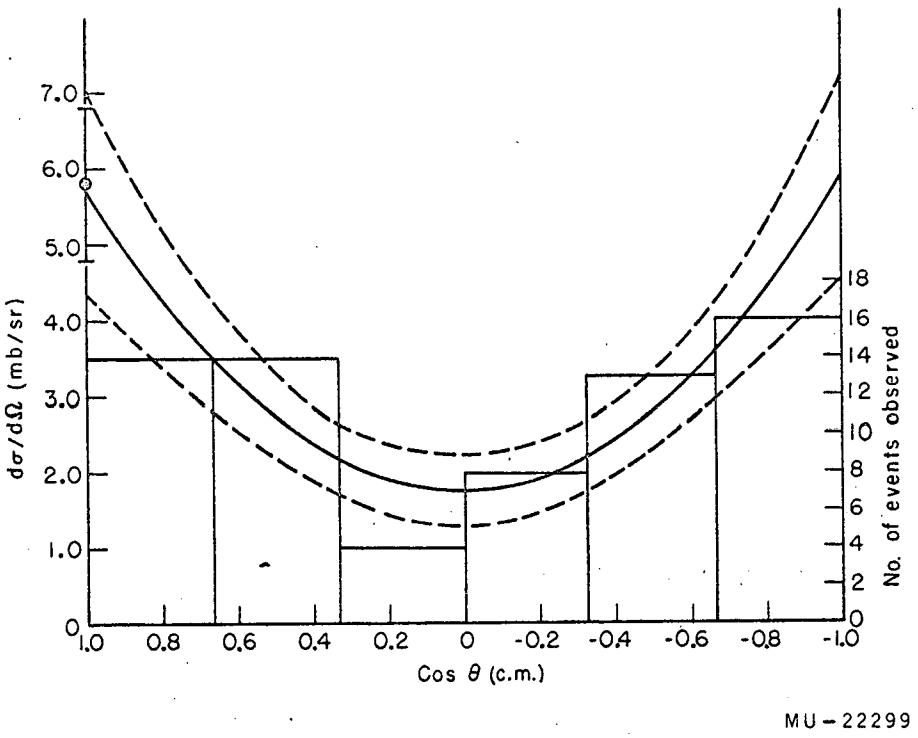
7.0
6.0
5.0
4.0
3.0
2.0
1.0
0
dσ/dΩ (mb/sr)
18
16
14
12
10
8
6
4
2
0
No. of events observed
1.0
0.8
0.6
0.4
0.2
0
-0.2
-0.4
-0.6
-0.8
-1.0
Cos θ (c.m.)
MU-22299

Fig. 8

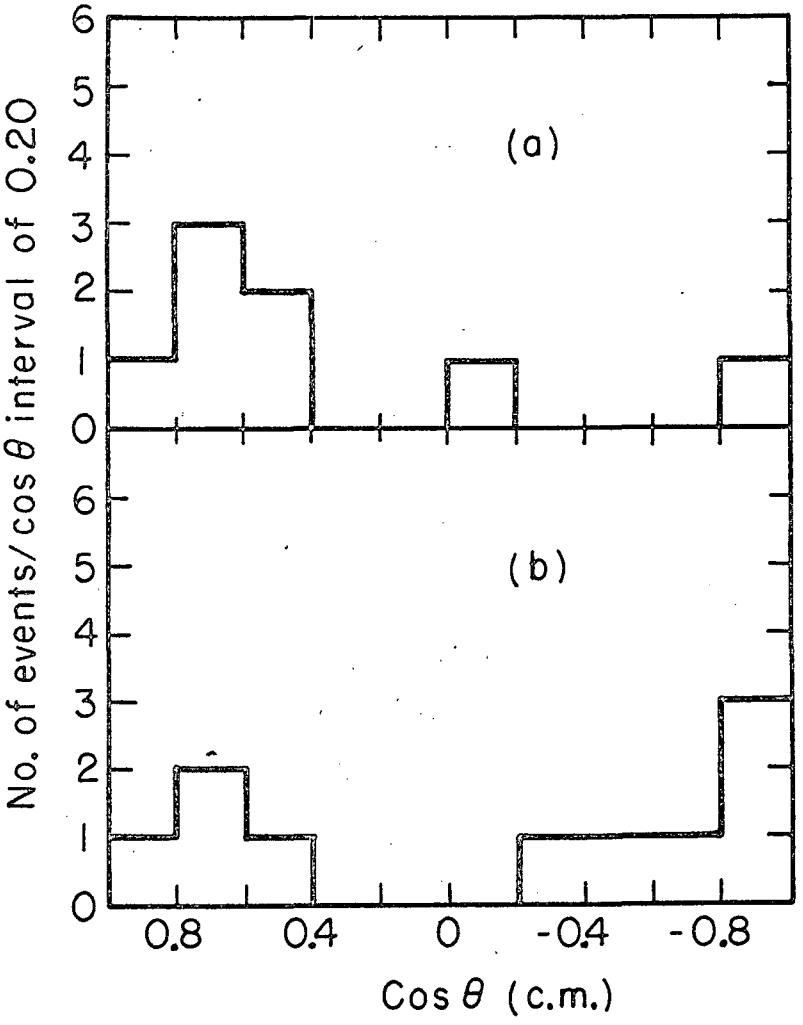


MU-22300

Fig. 9

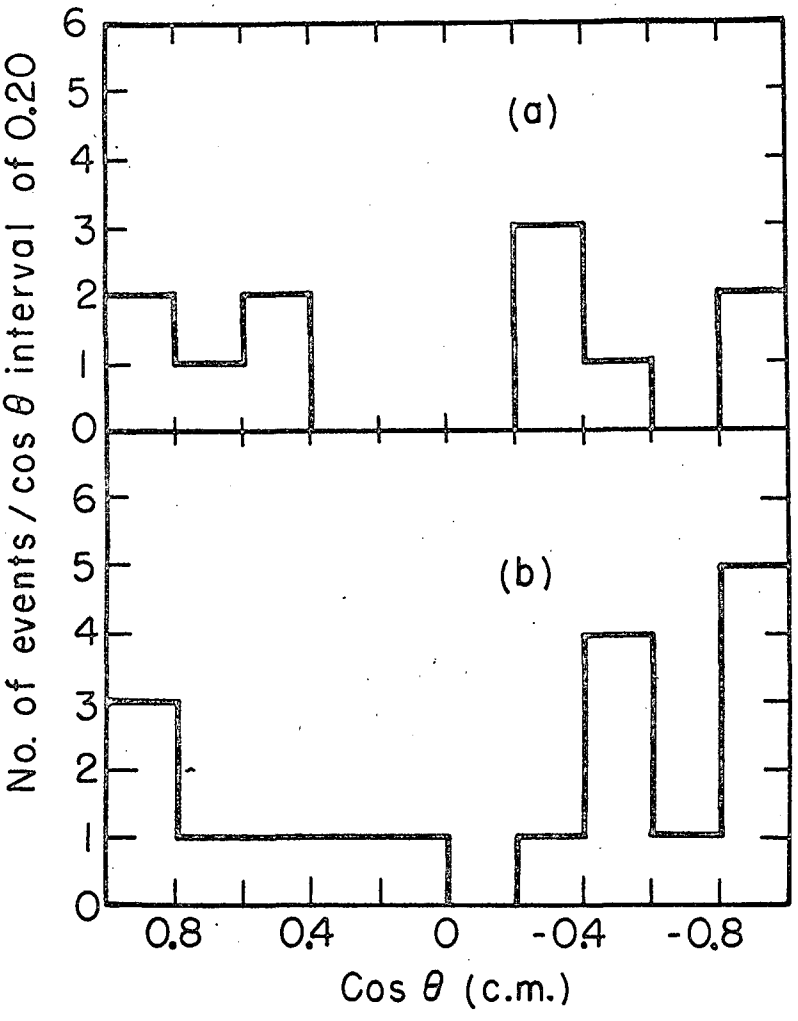


MU-22301

Fig. 10

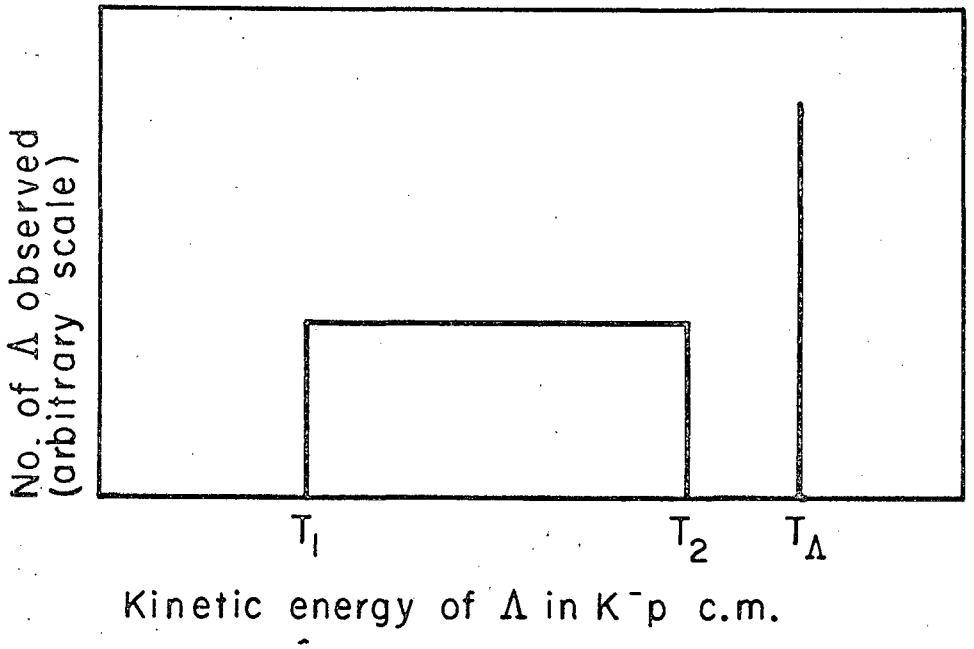


MU-22302

Fig. 11

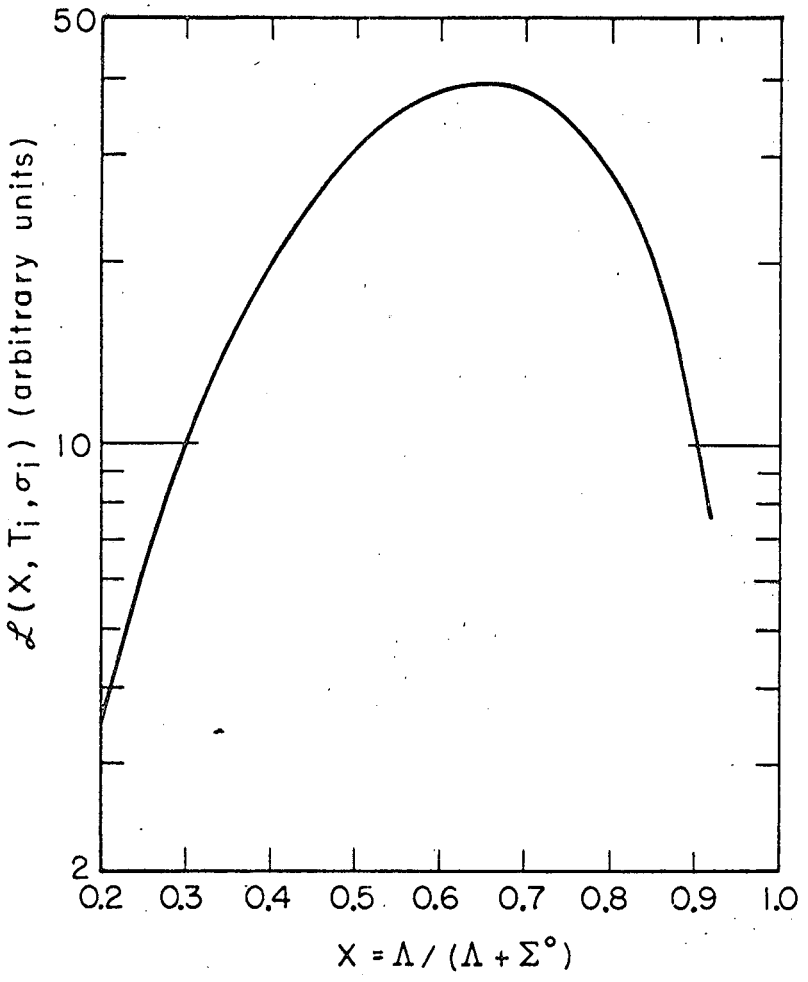
50
10
2
$\mathcal{L}(X, T_j, \sigma_j)$ (arbitrary units)
0.2
0.3
0.4
0.5
0.6
0.7
0.8
0.9
1.0
$X = \Lambda / (\Lambda + \Sigma^\circ)$
MU-22303

Fig. 12